Lab on a Chip

PAPER

View Article Online
View Journal | View Issue

Cite this: *Lab Chip*, 2020, **20**, 4205

Microengineered poly(HEMA) hydrogels for wearable contact lens biosensing†

Yihang Chen,[abc] Shiming Zhang,*[abde] Qingyu Cui,[f] Jiahua Ni,[abd] Xiaochen Wang,[abd] Xuanbing Cheng,[cg] Halima Alem,[abdhi] Peyton Tebon,[abd] Chun Xu,[abd] Changliang Guo,[f] Rohollah Nasiri,[abdj] Rosalia Moreddu,[kl] Ali K. Yetisen,[l] Samad Ahadian,[abd] Nureddin Ashammakhi,[abdm] Sam Emaminejad,[dg] Vadim Jucaud,[e] Mehmet R. Dokmeci[abem] and Ali Khademhosseini*[abdemn]

Microchannels in hydrogels play an essential role in enabling a smart contact lens. However, microchannels have rarely been created in commercial hydrogel contact lenses due to their sensitivity to conventional microfabrication techniques. Here, we report the fabrication of microchannels in poly(2-hydroxyethyl methacrylate) (poly(HEMA)) hydrogels that are used in commercial contact lenses with a three-dimensional (3D) printed mold. We investigated the corresponding capillary flow behaviors in these microchannels. We observed different capillary flow regimes in these microchannels, depending on their hydration level. In particular, we found that a peristaltic pressure could reinstate flow in a dehydrated channel, indicating that the motion of eye-blinking may help tears flow in a microchannel-containing contact lens. Colorimetric pH and electrochemical Na^+ sensing capabilities were demonstrated in these microchannels. This work paves the way for the development of microengineered poly(HEMA) hydrogels for various biomedical applications such as eye-care and wearable biosensing.

Received 3rd May 2020,
Accepted 4th September 2020

DOI: 10.1039/d0lc00446d

rsc.li/loc

Introduction

Noninvasive wearable biosensors[1] that can be used to detect biomarkers in bodily fluids, such as sweat, saliva, and tears, may one day replace some of the conventional medical instruments for various diagnostic applications.[2–5] Compared to sweat- and saliva-sensing, tear-sensing is a more competitive technology because the concentration of biomarkers in tears is reported to be more related to those in blood.[6] Besides, tears are less likely to be contaminated, and their sensing is less susceptible to other factors such as the secretion rate, evaporation, and temperature. Therefore, adding biosensing functions to commercial contact lenses, one of the most accepted wearable devices by the public, holds enormous commercial potential. For example, real-time monitoring of electrolyte concentration in tears, such as sodium ion (Na^+) concentration, could predict the occurrence of dry-eye disease.[7] Measuring pH changes in tears could reflect drug effectiveness and other clinical signs in disease processes,[8] while continuous monitoring of glucose concentration could help early diagnosis of diabetes.[9]

To avoid potential adverse effects on wearing comfort and to protect the sensing elements from delamination and contamination, contact lenses need to be micromachined to have encapsulated microchannels and

[a] *Center for Minimally Invasive Therapeutics (C-MIT), University of California-Los Angeles, Los Angeles, CA 90095, USA*
[b] *California NanoSystems Institute, University of California-Los Angeles, Los Angeles, CA 90095, USA*
[c] *Department of Materials Science and Engineering, University of California-Los Angeles, Los Angeles, CA 90095, USA*
[d] *Department of Bioengineering, University of California-Los Angeles, Los Angeles, CA 90095, USA. E-mail: szhang@eee.hku.hk, khademh@terasaki.org*
[e] *Terasaki Institute for Biomedical Innovation, Los Angeles, CA 90064, USA*
[f] *Department of Medicine, David Geffen School of Medicine, University of California, Los Angeles, CA 90095, USA*
[g] *Department of Electrical and Computer Engineering, University of California-Los Angeles, Los Angeles, CA 90095, USA*
[h] *Institut Jean Lamour, Université de Lorraine-CNRS, 54000 Nancy, France*
[i] *Institut Universitaire de France, France*
[j] *Department of Mechanical Engineering, Sharif University of Technology, Tehran, 11365-11155, Iran*
[k] *School of Chemical Engineering, University of Birmingham, Edgbaston, Birmingham B15 2TT, UK*
[l] *Department of Chemical Engineering, Imperial College London, South Kensington Campus, London SW7 2AZ, UK*
[m] *Department of Radiology, University of California-Los Angeles, Los Angeles, CA 90095, USA*
[n] *Department of Chemical and Biomolecular Engineering, University of California-Los Angeles, Los Angeles, CA 90095, USA*

† Electronic supplementary information (ESI) available. See DOI: 10.1039/d0lc00446d

microchambers. These encapsulated channels and chambers are ideal places where the biosensors can be integrated.

Further enabling a guided tear flow in these microchannels is essential to collect and to distribute tear fluid to specific sensing areas.[10,11] To date, several methods have been proposed for prototyping microchannels in contact lenses; however, they were mostly demonstrated with non-commercial materials such as silicone elastomers that are easy to micromachine.[12,13] Although the poly(2-hydroxyethyl methacrylate) (poly(HEMA)) hydrogel has excellent biocompatibility, softness, and transparency,[14–17] it is not compatible with mainstream microfabrication technologies. For example, soft lithography is compatible with polydimethylsiloxane (PDMS),[18] but it is not readily adaptable for molding highly viscoelastic hydrogels. Photolithography can be used to microfabricate tiny structures in elastomers, whereas it is challenging to use for hydrogels, which are susceptible to vacuum-, solvent-, and temperature-induced deformations. Dissolving and drying hydrogel powders in micromolds is preferred when fabricating patterned thin hydrogel membranes, yet it remains challenging to obtain complex 3D structures.[19,20] Laser ablation is another alternative, but it results in rough channel surfaces and non-uniform channel cross-sections.[21]

This work reports the micromachining of microchannels in poly(HEMA) hydrogels used for commercial contact lenses. A 3D printing technique was used to create reverse molds for these microchannels. A systematic experimental effort was dedicated to identifying an optimized process flow that allows the molding and delaminating the hydrogel from the 3D printed molds while maintaining smooth and well-defined channels after separation. Encapsulation of these microchannels was realized by either treating the hydrogel surface with plasma or using a non-crosslinked precursor as an adhesive layer. We performed a qualitative study to investigate the relationship between the flow behavior in these microchannels and the hydrogel hydration level. Significantly, we revealed that an external peristaltic pressure could reinstate flow in the dehydrated microchannels. This phenomenon indicates that the motion of eye-blinking might improve tear flow in a microchannel-containing contact lens. Colorimetric pH and electrochemical Na^+ biosensors were integrated into poly(HEMA) hydrogel channels, which are relevant to tear osmolarity monitoring and dry-eye disease prevention. These findings promote the use of commercial poly(HEMA) hydrogels for various biomedical applications such as eye-care and wearable biosensing.

Results and discussion

The poly(HEMA) hydrogel was synthesized by optimizing the concentrations of the monomer, 2-hydroxyethyl methacrylate (HEMA), the cross-linker, ethylene glycol dimethacrylate (EGDMA), and the thermal initiator, benzoyl peroxide (BP) in the precursor solution, as shown in Fig. 1A. The as-synthesized poly(HEMA) hydrogel exhibited a high contact angle (about 110°, as shown in Fig. 1B). The Young's modulus of the as-synthesized poly(HEMA) hydrogel was about 12 MPa (Fig. 1C). However, as expected,[22] after hydration in deionized water at room temperature, the modulus of the poly(HEMA) hydrogel quickly decreased to 1 MPa within 8 hours. The contact angle also reduced to ~60° due to an increased water content.[22,23] The poly(HEMA) hydrogel had a swelling ratio of ~1.5 after 24 hours of immersion in water at room temperature (Fig. 1D).[24,25]

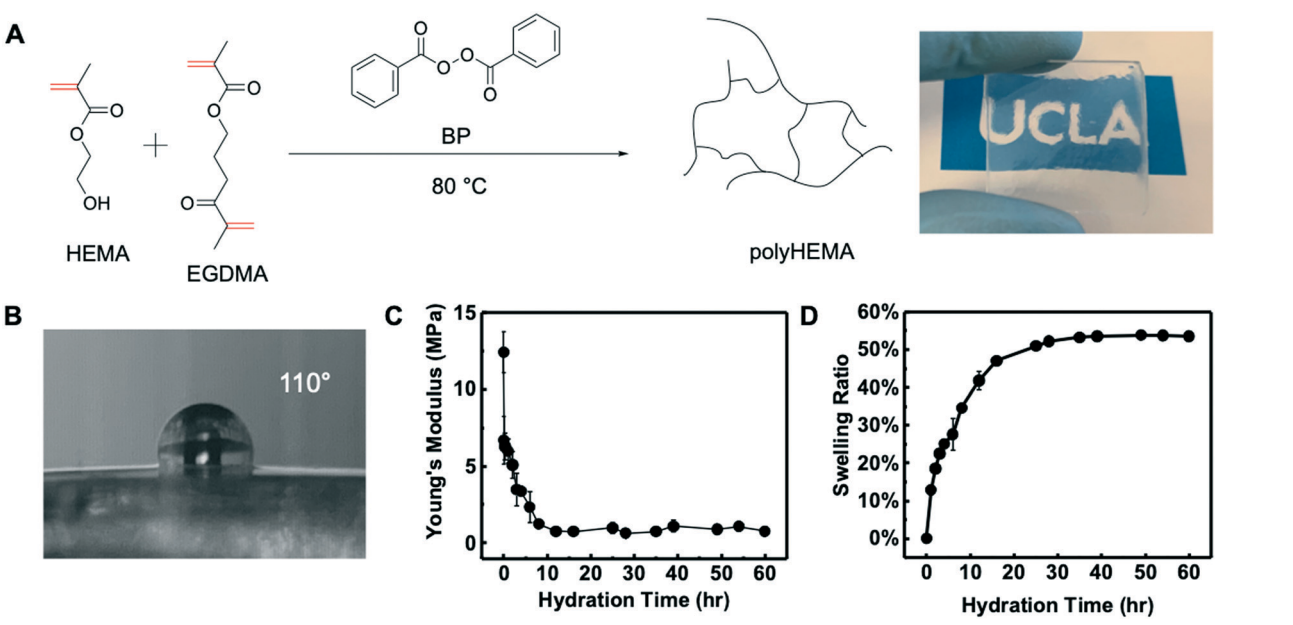

Fig. 1 Synthesis and characterization of the poly(HEMA) hydrogel. (A) Synthesis of the poly(HEMA) hydrogel (inset shows the transparent poly(HEMA) hydrogel); (B) contact angle measurement of the as-synthesized poly(HEMA) hydrogel; (C and D) the Young's modulus and swelling ratio change with increasing poly(HEMA) hydration levels.

The process flow of the fabrication of microchannels in the poly(HEMA) hydrogel is shown in Fig. 2A. High-resolution resin molds were printed with a 3D printer (with a resolution of 30 μm). A 2-μm parylene anti-adhesion layer was deposited on the mold to ease the future separation of the hydrogel from the mold after thermal crosslinking. Next, the poly(HEMA)

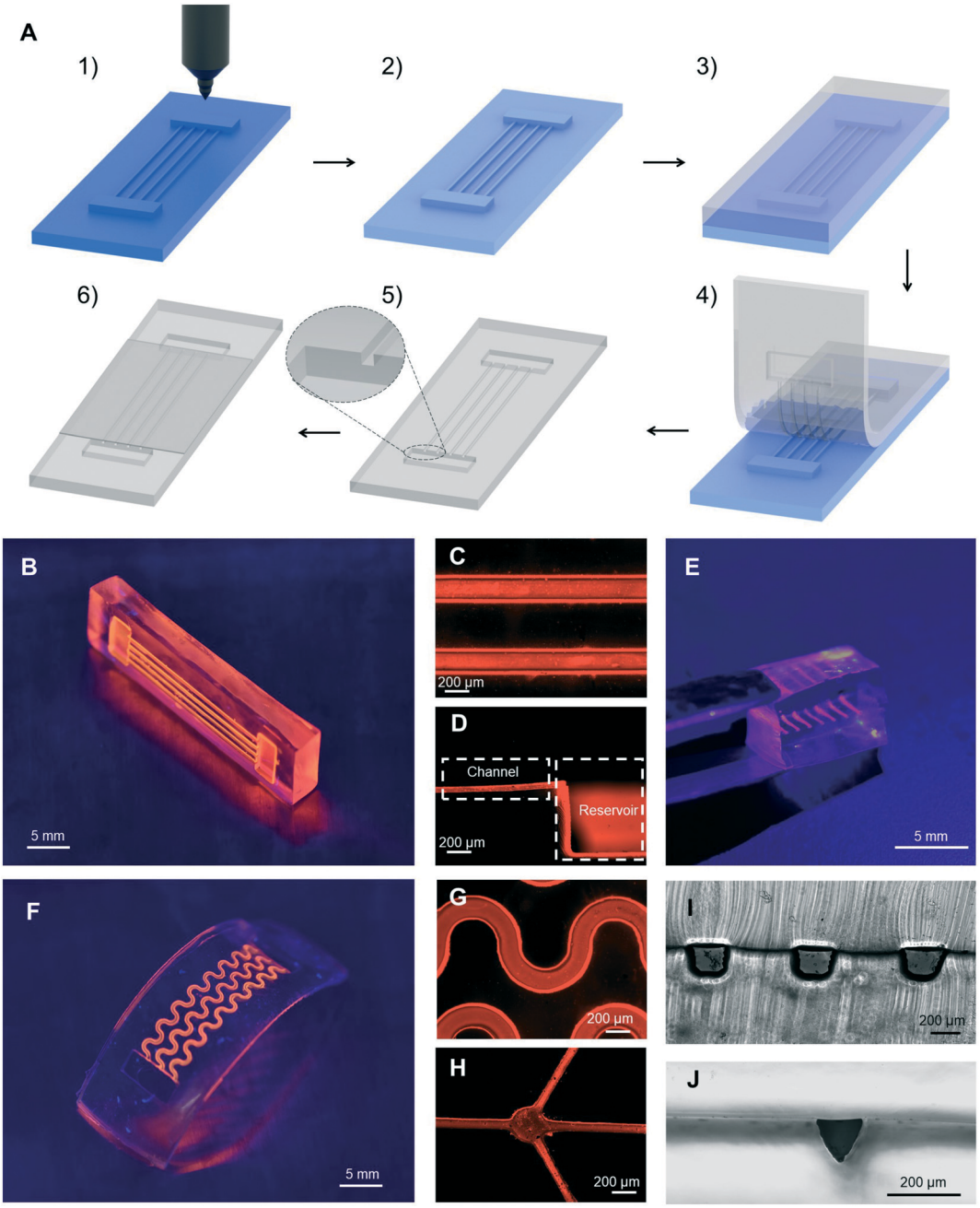

Fig. 2 Microfabrication of microchannels in the poly(HEMA) hydrogel. (A) Process flow of fabricating encapsulated microchannels in a poly(HEMA) hydrogel with the combination of 3D printing and replication. It includes: 1) 3D printing of a reverse mold; 2) deposition of a 2 μm-thick parylene layer on the mold to ease future removal; 3) casting the poly(HEMA) precursor on the mold; 4) removal of the poly(HEMA) hydrogel; 5) flattening of the micromachined poly(HEMA) hydrogel; 6) encapsulation of the poly(HEMA) microchannels with a thin poly(HEMA) capping layer. (B and C) Straight poly(HEMA) microchannels with a width and depth of 200 μm and poly(HEMA) reservoirs with a depth of 500 μm; (D) cross-section of the poly(HEMA) microchannel (100 μm in width and depth) connecting to a reservoir with a depth of 1 mm; (E) encapsulation of poly(HEMA) microchannels (bottom) with a poly(HEMA) capping layer (top) *via* plasma-assisted bonding (details in the Materials and methods section); (F and G) serpentine-shaped poly(HEMA) microchannels with a channel width of 200 μm; (H) poly(HEMA) microchannels with a reservoir connecting four branches in different directions; (I and J) cross-sectional images of the encapsulated poly(HEMA) microchannels (200 μm in depth). The demonstrated microchannels were obtained by 3D printing and plasma-assisted bonding (I) and laser ablation and poly(HEMA) precursor-assisted bonding (J), respectively.

precursor was cast onto the mold and polymerized (details in the Materials and methods section). After polymerization, the poly(HEMA) hydrogel showed strong adhesion to the mold and was not detachable. We resolved this critical issue by immersing the sample in hot water (80 °C) overnight. With this method, the poly(HEMA) hydrogel with smooth and well-defined microchannels could be delaminated from the mold, with a thickness as thin as 1 mm.

To encapsulate the microchannels created in the poly(HEMA) hydrogel, we developed the following two methods. In the first one, oxygen plasma was used to treat the surface of the poly(HEMA) hydrogels to promote the bonding of microchannel-containing poly(HEMA) with a thin poly(HEMA) capping layer. Under oxygen plasma exposure, the poly(HEMA) surface became hydrophilic due to the formation of radicals and alcohol, ester, carboxylic and carbonyl groups, similiar to the work describing the influence of plasma on poly(methyl methacrylate) (PMMA).[26] Indeed, both polymers' pending groups display similar chemical structures. Bonding of two poly(HEMA) layers together was performed immediately after plasma treatment to avoid any reorganization of the polymer chain at the surface of the poly(HEMA) layers. The newly formed low molecular weight chains, after the polymer chain scission by oxygen plasma, can migrate from the air–poly(HEMA) interface to the bulk of the material. The native polymer long chains move to the top surface by crawling, which generally leads to the initial surface energy recovery as shown for other polymers.[27,28] Regarding the poly(HEMA) hydrogel used in this work, the crawling kinetics slowed down due to the reticulated structure.

In the second bonding method, the precursor of the poly(HEMA) hydrogel was used as an adhesion promoter to crosslink two separate poly(HEMA) hydrogels together. In this method, the poly(HEMA) precursor was spin-coated on the microchannel-containing poly(HEMA) hydrogel. Immediately after spin-coating of the precursor solution onto the microchannel-containing hydrogel, the capping layer was pressed atop, followed by a full thermal crosslinking process in an oven. The second method is favorable towards a stronger bonding, whereas the first method is preferred when a dry encapsulation process is needed. Unless otherwise mentioned, the plasma-assisted dry encapsulation method was used throughout this work (Fig. 2E, I, and J).

Visualization of flows in the microchannel-containing poly(HEMA) hydrogels permits a qualitative study of flow dynamics. To ease the visualization, a smartphone was used as a recording camera (Fig. S1†).[29–32] This practical setup is portable and permits an easy adjustment of the camera lens to the desired directions. In this design, a 10× macro lens was integrated with the smartphone, which enabled a close flow visualization in the microchannels.

In short, we identified three flow stages in the microchannel-containing poly(HEMA) hydrogel, which are dependent on the hydrogel's hydration level (qualitatively summarized in Fig. 3A–D). In a dehydrated poly(HEMA) hydrogel, the surface was hydrophobic; therefore, no flow was observed (stage 1, Fig. 3A, and ESI† Video S1). In a fully hydrated poly(HEMA) hydrogel, we observed a Laplace pressure-driven spontaneous capillary flow (stage 3, Fig. 3D, and ESI† Video S2). Significantly, we repeatedly observed that a transition stage existed between the fully hydrated and dehydrated stages, where the ceased flow was reinstated after the application of an external peristaltic pressure (close to the pressure of eye-blinking) on the hydrogel capping layer (stage 2, Fig. 3B, and ESI† Video S3). The observations of peristaltic pressure-induced flow in the poly(HEMA) microchannels represent one of the key findings of this work. It indicates

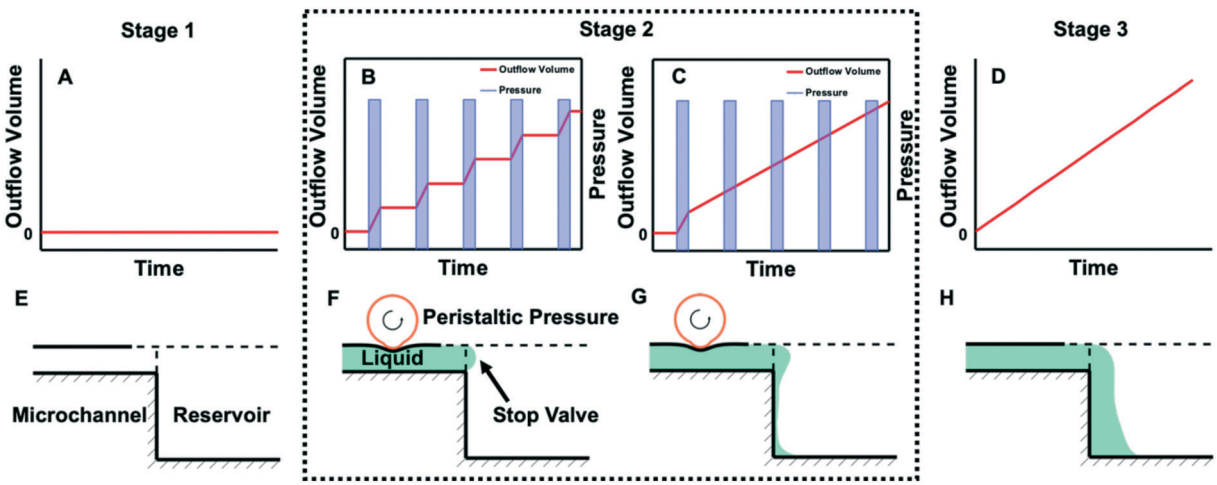

Fig. 3 Flow stages in poly(HEMA) microchannels, depending on the hydration level of poly(HEMA). (A–D) Illustration of the flow volume collected in the drain reservoir over time, and (E–H) illustration of the corresponding flow behavior. (A and E) No flow was observed in a fully dehydrated poly(HEMA) microchannel (dried with a nitrogen gun); (B and F) peristaltic pressure (mimicking eye blinking) induced flow in mildly hydrated poly(HEMA) microchannels; (C and G) transition from peristaltic pressure-induced flow to spontaneous capillary flow was observed after one more cycle of pressure; (D and H) spontaneous flow was observed directly in fully hydrated poly(HEMA) microchannels.

that eye-blinking pressure may help promote tear flow within the microchannel-containing poly(HEMA) contact lens. It also supports the idea of eye-blinking assisted biosensing studies using contact lenses to stimulate the development of smart contact lenses for eye-care and wearable biosensing. Noteworthily, the peristaltic pressure-driven flow in stage 2 could change to spontaneous flow after several pressure cycles (stage 2, Fig. 3C), which could be attributed to the increased hydration level of the hydrogel surface due to the inflow of the dye solution.

The reason that external peristaltic pressure was able to reinstate flow in stage 2 could be, at least partially, attributed to the abrupt geometric expansion at the junction between the microchannel and the drain reservoir (Fig. 2D and 3E–H). We surmised that when the flow meniscus reaches the channel/reservoir junction, the abrupt geometric change (in both channel width and depth) prevented the fluid meniscus to further advance. In this case, the application of an external peristaltic pressure repeatedly broke the established equilibrium state of the flow meniscus, which squeezed the liquid into the drain reservoir and helped establish a new equilibrium state. The stage of peristaltic pressure-induced flow was maintained until the junction became sufficiently hydrated to induce a significant Laplace pressure that could reinstate a spontaneous flow[9] (stage 3).

To evaluate the time required for the transition between the above-identified stages, we performed a time-varying flow visualization in these microchannels. In this experiment, we exposed the surface of a fully hydrated hydrogel to ambient air for different periods to dehydrate the sample. Fig. 4A shows the observed stages of the flow as a function of dehydration time. The results can be summarized as follows: i) spontaneous flow (stage 3) was maintained as long as the exposure time was less than 9 min; ii) spontaneous flow changed to pressure-induced flow (stage 2) when the exposure time was between 9 min and 15 min (started at

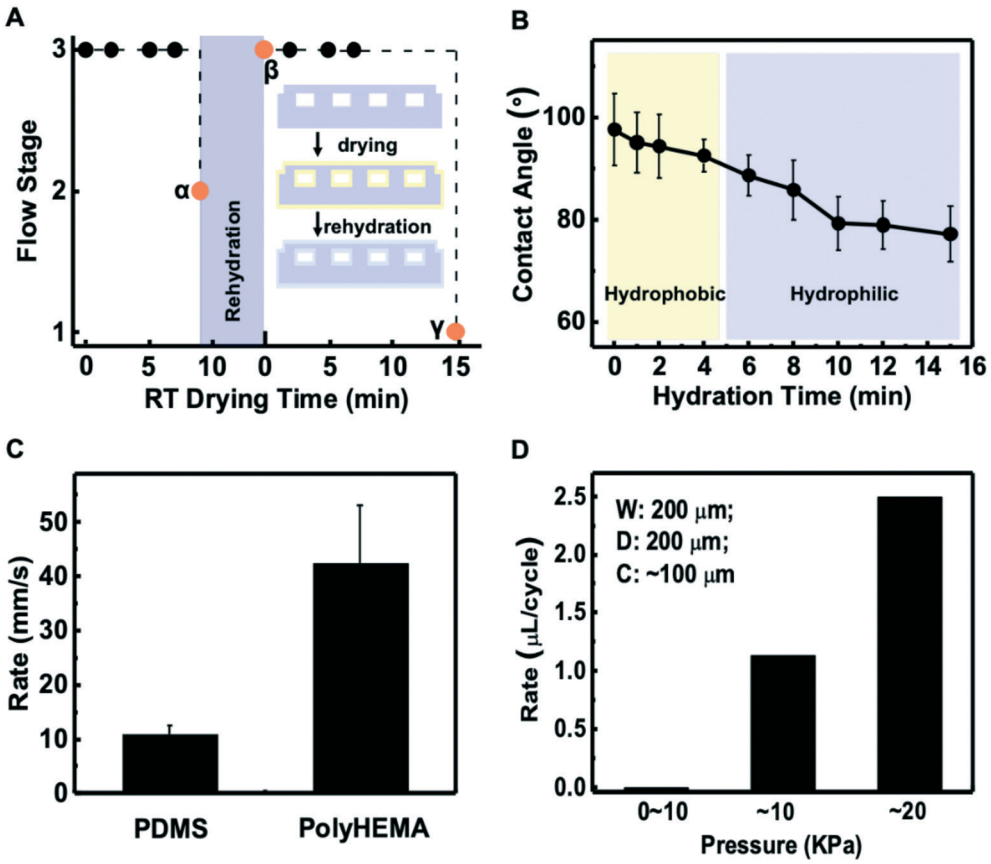

Fig. 4 A) Investigation of flow transition time from spontaneous capillary flow to pressure-activated flow, and no flow by dehydrating a fully hydrated hydrogel under ambient conditions. The shadow area indicates the transition from stage 2 to stage 3 (5 min rehydration, starting at point β) by re-hydrating the sample. The inset illustrates the dehydration and rehydration processes in the poly(HEMA) microchannels; B) contact angle change on a flat poly(HEMA) hydrogel surface with increased hydration time (N = 10, the measurements were performed in triplicate); the hydrogel was initially dehydrated with a nitrogen gun (2 min); C) comparison of the flow rates in PDMS microchannels and poly(HEMA) microchannels (with a channel width and depth of 200 μm). The flow rate in fully hydrated poly(HEMA) microchannels (~40 mm s^{-1}) was about four times faster than that in PDMS microchannels; D) increasing the peristaltic pressure increased the volume of the fluid delivered per pressure cycle (W/T/L of 200 μm/200 μm/16 mm). These results demonstrate that eye blinking may help flow exchange in the poly(HEMA) microchannels. The volumetric flow rate was estimated by measuring the increased volume of the fluid in the drain reservoir after each pressure cycle. The rate represents the average value of multiple pressure cycles.

point α, as shown in Fig. 4A); iii) the surface became hydrophobic, and no flow was observed (stage 1) when the exposure time was longer than 15 min (started at point γ, as shown in Fig. 4A). A contact angle of 100° was measured on a fully dehydrated and flat poly(HEMA) hydrogel surface, which decreased to 75° after water immersion for 15 min (Fig. 4B).

An accelerated flow rate in a microchannel is preferred for advanced microfluidic applications. The flow rate in the micromachined poly(HEMA) hydrogel microchannels is superior to that in a microchannel-containing elastomer. For example, the estimated flow rate in the poly(HEMA) hydrogel was about four times higher than that in PDMS microchannels with the same geometric profile (Fig. 4C, ESI† Video S4 (hydrogel) and S5 (PDMS)). We also qualitatively evaluated the volumetric flow rate per cycle as a function of applied pressure (stage 2, Fig. 4D). Upon applying a peristaltic pressure of ~10 kPa, a volumetric flow rate of ~1 μL per cycle was calculated, which increased to 2.5 μL per cycle when the pressure was increased to ~20 kPa. A quantitative study is encouraged to gain a deeper understanding of the dynamics. We are currently working on enabling the quantitative characterization of flow rates and dynamics by building a platform where the ambient humidity, the hydration level of the hydrogel, and peristaltic pressure can be simultaneously and precisely controlled.

The ameliorated flows in the hydrated poly(HEMA) hydrogel microchannels encourage their application for wearable contact lens biosensing. Therefore, we first created a prototype of a fully wearable untethered colorimetric pH sensor in these poly(HEMA) channels (Fig. 5). The pH value of tears has therapeutic and diagnostic significance.[8] The shift in pH values affects both cell viability and antibiotic effectiveness. Therefore, monitoring pH changes in tears can help in understanding the mechanisms of disease processes.[8] As shown in Fig. 5A, spontaneous flow occurred in the poly(HEMA) contact lens prototype where the channels were created (fully hydrated state, stage 3 in Fig. 3). The artificial tears of different pH values in the sampling chamber (Fig. 5B) could spontaneously flow into the storing reservoirs, and then to the sensing reservoirs through the contact lens' microchannels. The colorimetric pH indicator in the sensing chamber displayed different colors when interfacing with fluids of different pH values between 5 and 9 (Fig. 5C), which thoroughly cover the pH range of human tears (5–7.5).[8] The detection time of the colorimetric indicator was about 5 min.

To further validate the promise of using the microchannel-containing poly(HEMA) hydrogel for contact lens biosensing, we integrated a Na^+ electrochemical sensor in the poly(HEMA) hydrogel's microchambers. The concentration of Na^+ is an essential health indicator in tears that is relevant to tear

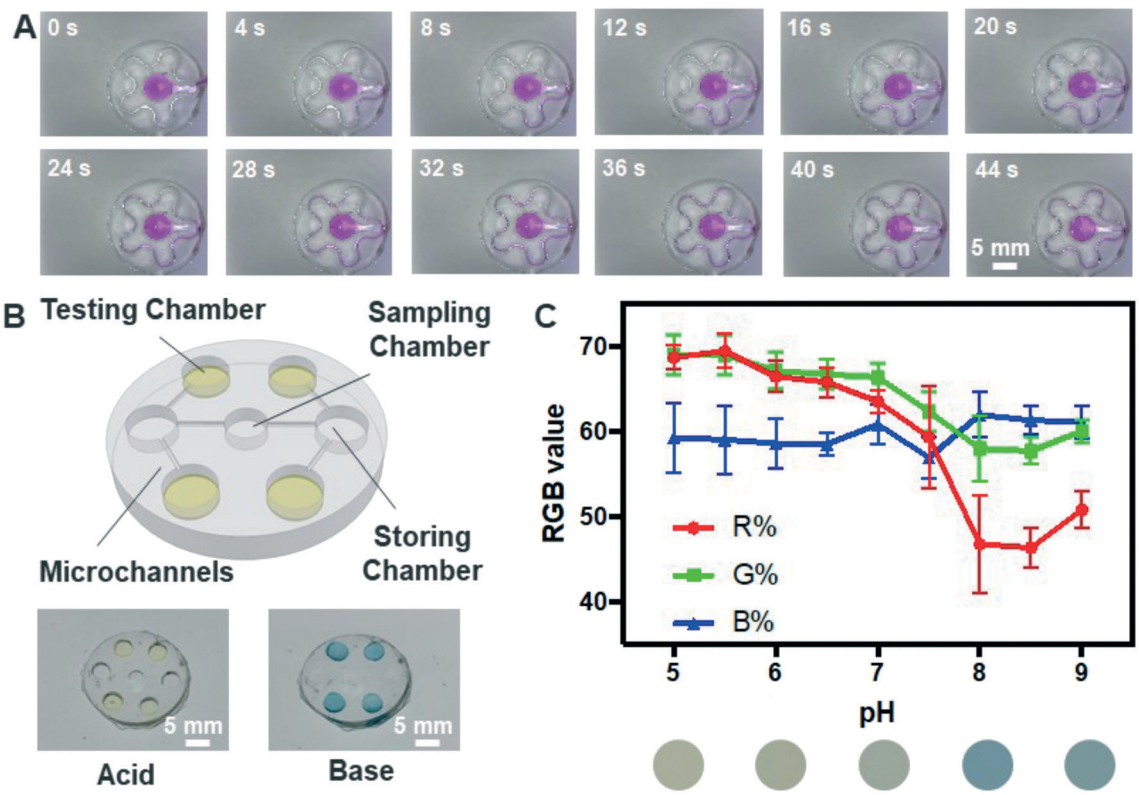

Fig. 5 Colorimetric contact lens biosensor in microchannel-containing poly(HEMA) contact lens. A) The flow administration in the microchannel-containing poly(HEMA) contact lens. B) The concept of the poly(HEMA) microchannel based contact lens biosensor. The bottom images show the real color response of the pH colorimetric sensor to acid and base solutions. C) RGB triplet of the biosensor at different pH values ranging from 5.0 to 9.0 with a step of 0.5 in aqueous solutions (N = 8). Inset shows the displayed color in the test chamber that was filled with target solutions.

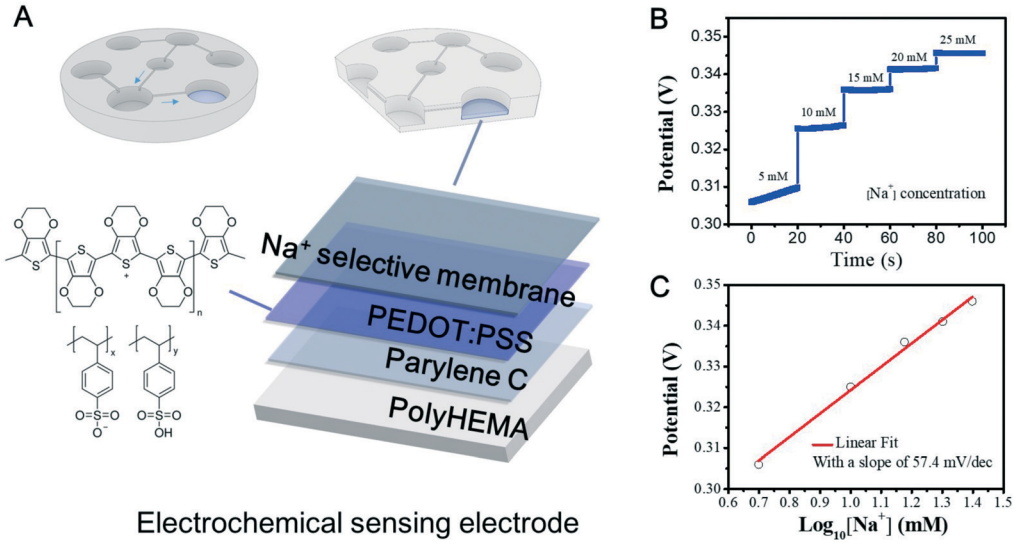

Fig. 6 Potentiometric Na^+ sensing electrode in poly(HEMA) hydrogel channels. A) The Na^+ electrochemical sensor was fabricated on a PEDOT:PSS coated Au/parylene-C film and then bonded to the poly(HEMA) reservoir. B) The open-circuit potential increased with increasing NaCl concentrations. C) A slope of 57.4 mV dec^{-1} was obtained, which was close to the theoretical value of 59 mV dec^{-1}.

osmolarity and dry-eye disease. The Na^+ selective membrane-containing poly(3,4-ethylenedioxythiophene) polystyrene sulfonate (PEDOT:PSS) electrode (deposited on a parylene substrate, Fig. 6A) could adhere firmly onto the hydrogel substrate by using the hydrogel precursor as an adhesive promoter. Fig. 6B shows the potential response of the Na^+ electrochemical sensor, potentiometrically measured in 5–25 mM NaCl solutions. The potential *versus* the Na^+ concentration followed a linear relationship with a slope of 57.4 mV dec^{-1}, which is in good agreement with the theoretically predicted value of 59.2 mV dec^{-1} (according to the Nernst equation at 25 °C). The detection range of the proposed Na^+ electrochemical sensor is relevant to tear osmolarity monitoring and dry-eye disease diagnosis.[13] It is envisioned that further integration of an untethered colorimetric Na^+ biosensor in a poly(HEMA) contact lens will promote its use for medical wearable applications.

Conclusion

In summary, we have demonstrated the fabrication of microchannel-containing poly(HEMA) hydrogels with high-resolution 3D printing and replica molding. These microchannels were encapsulated with either a plasma-assisted bonding method or a precursor-assisted bonding method. We qualitatively investigated the flow dynamics in the poly(HEMA) microchannels and found three flow regimes. Spontaneous Laplace pressure-driven capillary flow was observed in a fully hydrated sample. A peristaltic pressure-induced flow was observed in a mildly dehydrated sample. No flow was observed in a fully dehydrated sample. The observation of peristaltic pressure-driven flow is of importance because it indicates that eye-blinking pressure may help to promote tear flow in a microchannel-containing hydrogel contact lens. As a prototype for wearable biosensing, we further integrated colorimetric pH and electrochemical Na^+ biosensors into a poly(HEMA) hydrogel contact lens. This work places the poly(HEMA) hydrogel in the frontline for microfluidic and contact lens biosensing applications.

Materials and methods

Materials

HEMA, EGDMA, and BP were purchased from Sigma-Aldrich. Deionized (DI) water was obtained with Aqua Solutions lab water systems. PDMS (SYLGARD 184) was purchased from Dow Chemical Company. The resin used for 3D printing, B9R-1-Cherry, was obtained from B9Creations, LLC, and was used as received. Parylene C powder was purchased from Specialty Coating Systems Inc (SCS). PEDOT:PSS (Clevios™ PH1000) was purchased from Haraeus Electronic Materials, Germany. 4-Dodecylbenzenesulfonic acid (DBSA), glycerol (99.5+ % purity), and (3-glycidyloxypropyl)trimethoxysilane (GOPS) were purchased from Sigma-Aldrich. Sodium ionophore X (71747), bis(2-ethylhexyl) sebacate (DOS, 84822), sodium tetrakis[3,5-bis(trifluoromethyl)phenyl]borate (Na-TFPB, 692360), high-molecular-weight polyvinyl chloride (PVC) and tetrahydrofuran were purchased from Sigma-Aldrich. For flow visualization experiments, rhodamine B and tartrazine fluorescent dyes (Sigma-Aldrich) in deionized water were used. Bromothymol blue, methyl red, and phenolphthalein of the colorimetric pH sensing solution were purchased from Sigma-Aldrich and used without further purification.

Synthesis of poly(HEMA) hydrogels

Poly(HEMA) hydrogels were synthesized by free-radical polymerization of HEMA with 0.5 w/w% BP, as the free-radical initiator, and 1 v/v% EGDMA, as the crosslinking agent. For

example, 40.3 mg BP, 6 mL HEMA, and 61 μL EGDMA were added to a mixing tube. This hydrogel precursor mixture was vortexed and sonicated until there were no visible solids. The mixture was then filled into a mold and de-gassed to prevent cavity or bubble formation in the final poly(HEMA) hydrogel. The fully cross-linked hydrogel was obtained after thermal curing the precursor in an oven at 80 °C for 1 hour.

Characterization of the poly(HEMA) hydrogel

The contact angle of poly(HEMA) hydrogel was tested with a goniometer (AST VCA-3000S Wafer Surface Analysis System, USA). The modulus of the poly(HEMA) hydrogels was measured with an INSTRON tensile tester (INSTRON 5943, USA) in compression mode. The swelling ratio was tested by measuring the weight of poly(HEMA) before and after the immersion in DI water for varying time scales (0–60 hours). The original length, width, and height of the poly(HEMA) hydrogel were 10 mm, 10 mm, and 3 mm, respectively. $N = 3$ for all the experiments.

Fabrication of poly(HEMA) hydrogel microchannels

For the 3D-shaped poly(HEMA) channel fabrication, high-resolution molds were directly printed with a 3D printer (MONO3 DLP 3D Printer) with a resolution of 30 μm. The mold was designed by computer-aided design (CAD) software. In this study, the microchannels' width was 100 or 200 μm, the depth was 100 or 200 μm, and the axial length was 16 mm. To ease the poly(HEMA) hydrogel delamination, a 2 μm thick parylene-C layer was deposited on the 3D printed mold using an SCS parylene deposition system. Next, the poly(HEMA) precursor was cast onto the mold and polymerized as described above. After polymerization, the poly(HEMA) hydrogel adhered firmly to the 3D printed mold. The hydrogel and mold were immersed in water (80 °C) overnight to ease delamination. After removing the fully hydrated poly(HEMA) hydrogel from the oven, the hydrogel, with well-defined microchannels, was gently delaminated from the mold. The thickness of the poly(HEMA) hydrogel ranged from 1 to 5 mm, depending on the volume of the HEMA precursor used. The final thickness of the crosslinked hydrogel was close to the height of the HEMA precursor solution that was placed in the hollow PDMS mold. That is, the hydrogel did not show significant shrinkage in terms of thickness after thermal crosslinking.

Encapsulation of poly(HEMA) hydrogel microchannels

The thin poly(HEMA) hydrogel capping layer was fabricated by injecting the precursor into a PDMS mold, followed by a thermal crosslinking process. To create the PDMS mold, poly(methyl methacrylate) (PMMA) was laser ablated to the desired shape (VLS 2.30, Universal Laser, USA). PDMS (10 : 1, SYLGARD 184) was poured onto a Petri dish containing the PMMA mold. The sample was then cured in an oven at 80 °C for 1 hour. Planar and concave PDMS sheets were then bonded together after being treated with oxygen plasma (2 min, oxygen flow rate of 35 cc min^{-1}, and power of ~120 W (PE-25, Plasma Etch Inc., USA)). Next, the poly(HEMA) precursor was injected into the PDMS mold, followed by a manual de-gassing process *via* syringe extraction. The sample was then placed in an 80 °C oven for 1 hour. After polymerization, the PDMS mold was manually separated, and the sample was immersed in water overnight in an 80 °C oven to enable the delamination of the poly(HEMA) hydrogel capping layer from PDMS.

To encapsulate these microchannels, the following two methods were used. In the first method, the surfaces of the hydrated microchannel-containing hydrogel and capping layer were both dried using a nitrogen gun, followed by oxygen plasma treatment for 2 min (10 cc min^{-1}, 160 W). Immediately after plasma treatment, the microchannel-containing hydrogel and capping layer were first pressed together for 1 min and then placed in an 80 °C oven (1 hour) to further enhance the adhesion. In the second bonding method, the surface of the capping layer was dried with a nitrogen gun before loading onto a spin-coater (WS-650-23B spin-coater).[33] Approximately 20 μL of the poly(HEMA) precursor was spin-coated on the poly(HEMA) hydrogel capping layer (500 rpm for 10 s, followed by 2000 rpm for 30 s). The microchannel-containing poly(HEMA) hydrogel was then dried with nitrogen gas and pressed onto the precursor-coated poly(HEMA) capping layer, followed by a heating process (80 °C oven for 1 hour) for crosslinking.

Flow visualization

Flow visualization in the microchannels was recorded *via* a smartphone camera (iPhone XR) integrated with a 10× macro lens. The smartphone was mounted on a *z*-stage to ease the position adjustment. The portable visualization setup allowed an easy adjustment of the camera lens to the desired direction. The peristaltic pressure application was enabled by the use of a speed controller (Oriental Motor BMUD30, USA), a motor (Oriental Motor BLM230HP, USA), a laser-ablated convex head, a *z*-stage, and a balance (as described in Fig. S1†). The motor speed was adjustable between 1 and 100 rpm. The PMMA convex heads were designed to have the shape of barrels (2 cm in diameter and 3 mm in length) with bumps of different angles obtained by laser ablation (VLS 2.30, Universal Laser, USA). Adjustment of the *z*-stage height controlled the applied force of the convex heads to the poly(HEMA) hydrogel capping layer. The pressure applied to the capping layer was estimated by the following equation:

$$P = \frac{mg}{A}$$

where m is the peak weight recorded by the underlying balance, g is the gravitational acceleration, and A is the contact area between the convex PMMA head and the capping layer.

Fabrication of the colorimetric sensor and electrochemical sensor onto poly(HEMA) hydrogels

The colorimetric pH indicator was prepared by mixing bromothymol blue (139 μg), methyl red (12 μg), and

phenolphthalein (86 μg) in 100 μL of deionized water. The solution was loaded directly into the poly(HEMA) testing chambers, after gentle resuspension. The sample was then placed in a desiccator for degassing (4 hours) to immobilize the pH colorimetric indicator into the poly(HEMA) testing chambers. Then, the sample was immersed in water (>2 hours) to fully hydrate the poly(HEMA) hydrogel. For pH indication, the analyte (pH from 5.0 to 9.0, step: 0.5) was loaded into the testing chambers. The color of the indicator was recorded about 5 min after reacting with the analyte.

The Na^+ selective electrochemical sensing electrode was obtained through the mixing of Na ionophore X (1%, w/w), DOS (65.45% w/w), PVC (33% w/w), and Na-TFPB (0.55% w/w). Next, 100 mg of the mixture was thoroughly dissolved in 660 μL of tetrahydrofuran.[4] The ion-selective sensing electrode was prepared by drop-casting 20 μL of the mixture onto PEDOT:PSS film (100 nm)/Au (100 nm)/parylene C (2 μm). The modified electrode was dried in air for 6 hours. The parylene C film was obtained through chemical vapor deposition with SCS coating systems. PEDOT:PSS (0.5 v/v% DBSA, 5 v/v% glycerol, and 1 v/v% GOPS) was spin-coated on the parylene C film at 2000 rpm (30s). The Na^+ selective electrode on the parylene C film was attached to the poly(HEMA) hydrogel by using poly(HEMA) precursors as adhesion promoters. Full crosslinking of the precursors increased the parylene C film adhesion to the poly(HEMA) hydrogel. The measurement was performed with an electrochemical workstation (CH Instruments), where Ag/AgCl was used as the reference electrode and a Pt wire was used as a counter electrode. A chronopotentiometry method was used for data collection without applying a current between the working electrode and the counter electrode.

Statement of contributions

Y. C. and S. Z. contributed equally to this work. Y. C. and J. N. synthesized the poly(HEMA) hydrogel. Y. C., J. N., and S. Z. visualized the flow behavior in the microchannels. Y. C. fabricated the encapsulated microchannels and investigated the hydration of the poly(HEMA) microchannels. H. A. analyzed the bonding mechanism of poly(HEMA) with plasma treatment. R. M. and A. Y. synthesized the pH colorimetric indicator. S. Z., X. C. and S. E. synthesized the Na^+ selective membrane and fabricated the Na^+ electrochemical sensor. Y. C., S. Z., Q. C., P. T., C. X., C. G., R. N., S. A., N. A., and V. J. revised the manuscript. S. Z. and Y. C. drafted the manuscript. S. Z. and A. K. supervised the whole research.

Conflicts of interest

The authors declare no conflict of interest.

Acknowledgements

The authors are grateful to Dr. Sourav Saha and Dr. Lu Jiang at the Advanced Development Center of CooperVision, Inc. for fruitful discussions in designing the experiments and constructive comments on the manuscript. This work is supported by a grant from CooperVision, Inc. A. K. Y. thanks the Engineering and Physical Sciences Research Council (EPSRC) for a New Investigator Award (EP/T013567/1).

References

1 S. Zhang, H. Ling, Y. Chen, Q. Cui, J. Ni, X. Wang, M. C. Hartel, X. Meng, K. Lee, J. Lee, W. Sun, H. Lin, S. Emaminejad, S. Ahadian, N. Ashammakhi, M. R. Dokmeci and A. Khademhosseini, *Adv. Funct. Mater.*, 2020, **30**, 1906016.
2 Y. Sekine, S. B. Kim, Y. Zhang, A. J. Bandodkar, S. Xu, J. Choi, M. Irie, T. R. Ray, P. Kohli, N. Kozai, T. Sugita, Y. Wu, K. Lee, K.-T. Lee, R. Ghaffari and J. A. Rogers, *Lab Chip*, 2018, **18**, 2178–2186.
3 J. Kim, A. S. Campbell, B. E.-F. de Ávila and J. Wang, *Nat. Biotechnol.*, 2019, 1.
4 W. Gao, S. Emaminejad, H. Y. Y. Nyein, S. Challa, K. Chen, A. Peck, H. M. Fahad, H. Ota, H. Shiraki and D. Kiriya, *Nature*, 2016, **529**, 509–514.
5 S. Zhang and F. Cicoira, *Nature*, 2018, **561**, 466–467.
6 S. H. Lee, Y. C. Cho and Y. Bin Choy, *Sci. Rep.*, 2019, **9**, 4747.
7 Y. Yang and W. Gao, *Chem. Soc. Rev.*, 2019, **48**, 1465–1491.
8 W. H. Coles and P. A. Jaros, *Br. J. Ophthalmol.*, 1984, **68**, 549–552.
9 J. Park, J. Kim, S.-Y. Kim, W. H. Cheong, J. Jang, Y.-G. Park, K. Na, Y.-T. Kim, J. H. Heo and C. Y. Lee, *Sci. Adv.*, 2018, **4**, eaap9841.
10 S. W. Choi and J. Kim, *Materials*, 2018, **11**, 1125.
11 R. Moreddu, D. Vigolo and A. K. Yetisen, *Adv. Healthcare Mater.*, 2019, **8**, 1900368.
12 J. Kim, E. Cha and J. U. Park, *Adv. Mater. Technol.*, 2020, **5**, 2070004.
13 R. C. Tseng, C.-C. Chen, S.-M. Hsu and H.-S. Chuang, *Sensors*, 2018, **18**, 2651.
14 C. S. A. Musgrave and F. Fang, *Materials*, 2019, **12**, 261.
15 M. F. Refojo, *J. Polym. Sci., Part A-1: Polym. Chem.*, 1967, **5**, 3103–3113.
16 B. D. Ratner and I. F. Miller, *J. Polym. Sci., Part A-1: Polym. Chem.*, 1972, **10**, 2425–2445.
17 A. J. Cadotte and T. B. DeMarse, *J. Neural Eng.*, 2005, **2**, 114–122.
18 Y. Xia and G. M. Whitesides, *Annu. Rev. Mater. Sci.*, 1998, **28**, 153–184.
19 Y.-C. Chen, Z. Zhang, S. Fouladdel, Y. Deol, P. N. Ingram, S. P. McDermott, E. Azizi, M. S. Wicha and E. Yoon, *Lab Chip*, 2016, **16**, 2935–2945.
20 Y.-C. Chen, P. N. Ingram, S. Fouladdel, S. P. McDermott, E. Azizi, M. S. Wicha and E. Yoon, *Sci. Rep.*, 2016, **6**, 27301.
21 M. Imran, R. A. Rahman, M. Ahmad, M. N. Akhtar, A. Usman and A. Sattar, *Laser Phys.*, 2016, **26**, 096101.
22 G. Su, T. Zhou, Y. Zhang, X. Liu and A. Zhang, *Soft Matter*, 2016, **12**, 1145–1157.
23 A. Y. Kwok, G. G. Qiao and D. H. Solomon, *Polymer*, 2004, **45**, 4017–4027.
24 C.-D. Young, J.-R. Wu and T.-L. Tsou, *J. Membr. Sci.*, 1998, **146**, 83–93.

25 T. Canal and N. A. Peppas, *J. Biomed. Mater. Res.*, 1989, **23**, 1183–1193.
26 S. B. Amor, G. Baud, M. Jacquet, G. Nanse, P. Fioux and M. Nardin, *Appl. Surf. Sci.*, 2000, **153**, 172–183.
27 M. Morra, E. Occhiello, R. Marola, F. Garbassi, P. Humphrey and D. Johnson, *J. Colloid Interface Sci.*, 1990, **137**, 11–24.
28 R. Williams, D. Wilson and N. Rhodes, *Biomaterials*, 2004, **25**, 4659–4673.
29 A. W. Martinez, S. T. Phillips and G. M. Whitesides, *Proc. Natl. Acad. Sci. U. S. A.*, 2008, **105**, 19606–19611.
30 S. Wang, X. Zhao, I. Khimji, R. Akbas, W. Qiu, D. Edwards, D. W. Cramer, B. Ye and U. Demirci, *Lab Chip*, 2011, **11**, 3411–3418.
31 A. F. Coskun, J. Wong, D. Khodadadi, R. Nagi, A. Tey and A. Ozcan, *Lab Chip*, 2013, **13**, 636–640.
32 A. K. Yetisen, J. L. Martinez-Hurtado, A. Garcia-Melendrez, F. da Cruz Vasconcellos and C. R. Lowe, *Sens. Actuators, B*, 2014, **196**, 156–160.
33 Y.-C. Chen, P. N. Ingram, S. Fouladdel, S. P. McDermott, E. Azizi, M. S. Wicha and E. Yoon, *Sci. Rep.*, 2016, **6**, 27301.